Structure of liquid GaSb at pressures up to 20 GPa

T. Hattori, K. Tsuji, N. Taga, Y. Takasugi, and T. Mori
Department of Physics, Keio University, Yokohama 223-8522, Japan
(Received 25 June 2003; published 12 December 2003)

We have investigated the structure of liquid GaSb up to 20 GPa by a high-pressure and high-temperature x-ray-diffraction technique. With increasing pressure, the hump at high-Q side of the first peak in the structure factor, $S(Q)$, reflecting an anisotropic local structure becomes smaller and the ratio of the wave number of the second peak to that of the first one, Q_2/Q_1, decreases. Simultaneously, the coordination number CN increases in correspondence to the elongation of the nearest-neighbor distance compared to that expected from a uniform contraction model. These findings suggest that the liquid GaSb contracts nonuniformly and the local structure changes with pressure. Analysis of the pair distribution function $g(r)$ by a distorted-crystalline model shows that the liquid consists of two parts similar to the β-Sn and body-centered cubic (bcc) structures which are realized in the high-pressure crystalline phases, rather than the zinc-blende structure in an ambient phase. The fraction of the bcc-like local structure increases continuously from 0.08 ± 0.05 to 0.43 ± 0.05 as the pressure is raised from 1.7 GPa to 20 GPa. The pressure dependence can be explained quantitatively by Rapoport's two-species model [J. Chem. Phys. **46**, 2891 (1967)]. The observed elongation of the nearest-neighbor distance and the increase of CN would be attributed to the continuous change of the local structure from the β-Sn-like one into the bcc-like one under pressure.

DOI: 10.1103/PhysRevB.68.224106 PACS number(s): 61.20.Qg, 61.10.Eq, 07.35.+k

I. INTRODUCTION

Application of pressure on crystals or liquids changes their structure drastically. But since the two phases have different degrees of allowance for the variation of the bond length and bond angle, they show different high-pressure behaviors; namely, the crystalline phases usually show drastic structural changes with a large volume jump, while the liquid phases do not show such a drastic structural change except for a few cases.[2] The transition pressure and the local structures of two phases are also different from each other. To understand the characteristic features of structural change in liquid, the structural investigations at high pressures is necessary.

Structural changes of crystalline phases under pressure are intensively studied. Specifically, the tetrahedrally bonded materials, such as group IV elements, III-V and II-VI compounds, have attracted much attention because of their interesting changes in the chemical bonding and in electric properties induced by pressure. Sequences of crystalline phases which appear on increasing pressure can be summarized as follows.[3] For elements or compounds with smaller ionic characters, the crystalline phases change from the diamond (or zinc-blende) structure into the β-Sn structure and/or the related orthorhombic *Imma* structure, and then into the simple hexagonal (SH) structure or the related orthorhombic *Ammm* structure,[4] and then into the close-packed structures, such as the face-centered-cubic (fcc) structure, hexagonal close-packed (hcp), and body-centered-cubic (bcc) structures. For those with a larger ionic character, the crystalline phases transform from the zinc-blende structure into the NaCl and/or the related orthorhombic *Cmcm* structures (sometimes through the cinnabar structure) with increasing pressure. Each transition is accompanied by the discontinuous volume change. Compared to these detailed studies on crystalline phases, the high-pressure structural changes in the liquid state are not well known because of experimental difficulties. Among a few studies are those on the pressure-dependent structures for liquid Si (l-Si) and liquid Ge (l-Ge).[5,6] It is reported that the local structure of l-Si drastically changes under pressure within the relatively small pressure interval. Contrary to l-Si, the local structure of l-Ge gradually changes over a wide pressure region.[6,7] On the other hand, the high-pressure behaviors of the liquid of the tetrahedrally bonded materials with an ionic character, such as III-V and II-VI compounds, have not been reported so far. Investigation on these compounds is expected to show the effect of ionicity on the local structure, and also information on the chemical ordering in binary liquids under pressure. In this study, we focused on the high-pressure behavior of liquid GaSb (l-GaSb) which has a least ionic character among III-V compounds.[8] We have investigated the local structure and the contraction process of l-GaSb under pressure up to 20 GPa by x-ray diffraction using synchrotron-radiation source in conjunction with the recently developed high-pressure experimental technique.[9,10]

For the later discussion, the pressure and temperature phase diagram for GaSb,[11,12] which has been reported previously, is shown in Fig. 1. Zinc-blende-type GaSb crystalline phases is stable at ambient condition. It transforms into a liquid metal on melting at high temperatures, similarly to Si and Ge. The transition is accompanied with the volume decrease.[13] It is anomalous because the volume of simple liquids, such as liquid alkali metals and van der Waals liquids, increases on melting. As for the high-pressure phases for the crystalline GaSb (c-GaSb), there is still a controversy. It has been reported that the zinc-blende structure transforms into the site-disordered β-Sn structure at 6.2 GPa,[14,15] then into the SH structure at 28 GPa, and then into an unidentified structure at 61 GPa.[16] Recently, it has been reported that the zinc-blende-type GaSb transforms into a site-disordered orthorhombic phase with the symmetry of

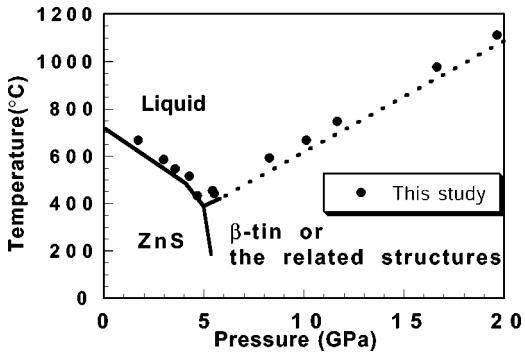

FIG. 1. Previously reported phase diagram for GaSb (Refs. 12 and 11) and the experimental PT conditions in this study. Phase boundary shown by bold line is after Ref. 11. The dotted line is the melting curve extrapolated from the melting curve between 5 and 6 GPa.

Imma at 7 GPa (Ref. 17) instead of the β-Sn and the SH structures, and then into a site-disordered orthorhombic *Ammm* phase at high pressures and temperature above 20 GPa and 473 K, respectively.[4] This discrepancy originates both from the different resolution of an x-ray-diffraction pattern and from the different hydrostatic condition.[18]

II. EXPERIMENT

The structure of *l*-GaSb was investigated by an energy-dispersive x-ray diffraction (EDX) method using a synchrotron-radiation source in conjunction with multianvil high-pressure apparatuses. For the collection of the data below 10 GPa, the single-stage high-pressure apparatus MAXIII installed at BL-14C2 in the High Energy Accelerator Research Organization (Photon factory, KEK) was used. For collection of the data above 10 GPa, the Kawai-type double-stage high-pressure apparatus SPEED1500 (Ref. 10), installed at BL04B1 in the SPring-8 was used. The diffraction intensity from the sample was collected by a pure Ge solid-state detector. Reagent-graded GaSb with a purity of 99.999% (Rare metallic Co., Ltd.) was used as a sample. To avoid too heavy x-ray absorption by the sample, we mixed NaCl with the sample so that μt becomes equal to 2 for the x-ray energy $E=40$ keV, where μ is the averaged linear absorption coefficient for GaSb and t is the sample thickness. The cell assemblies used in the high-pressure experiments were the same as those described in Refs. 19 and 9. We took the diffraction profiles at various 2θ angles to obtain $S(Q)$ over a wide Q region.[20]

The diffraction intensity was taken at high-PT conditions along the melting curve as shown in Fig. 1. The melting curve above 6 GPa was estimated from the data at the lower pressures[11] because the melting curve above 6 GPa has not been reported yet. Pressure was determined from the lattice parameter of the pressure marker (NaCl) on the basis of the equation of state.[21] Temperature is estimated from the electric power applied to the heater. The relation is checked beforehand. The accuracy in the determination of the pressure and the temperature was within 0.7 GPa and 100 K.

Most of the x-ray-diffraction peaks from the sample container (NaCl) were eliminated by a sharp slit system. However, a few peaks from the sample container and a dilution material of sample (NaCl) contaminated the x-ray-diffraction profile of the liquid. These peaks were eliminated from the raw data. We can easily perform the procedure because these peaks were sharp enough to distinguish them from the intensity profile of the liquid.[22] We corrected the absorption of x ray by the sample and the container, taking account of 2θ dependence of x-ray pass length. The data taken by EDX method show complex profiles due to the effects of the energy profile of the incident beam and the energy dependence of the quantum efficiency of the detector. Therefore, we have to connect the data taken at various angles after the collection of these effects. This procedure was carried out automatically by using the computer program coded by one of the authors (T.H.). The procedure is based on the empirical procedure described in Ref. 19, but the Compton scattering term was added to their formulas in this study. The algorithm of the program is as follows. First, the data taken at several 2θ angles are normalized by dividing the hypothetical $C(E)$ function which was defined from both the energy profile of the incident beam and the energy dependence of the quantum efficiency of the detector. These data are scaled and connected to each other so that the data overlap in the connected Q region. On the basis of the connected data, we made a hypothetical $S(Q)$. The $C(E)$ function for each angle is estimated again from this $S(Q)$ by the inversion procedure and the better $C(E)$ function is estimated. By iteration of these procedures, the optimum $C(E)$ function, which makes the data for several 2θ angles overlap most successfully, and the optimum $S(Q)$ are obtained. Any significant difference was not observed in the overlapped Q region (3 % at maximum). The atomic scattering factor was taken from Ref. 23. The Compton scattering factor were taken from Refs. 24 and 25. The profile of $S(Q)$ was deduced from the coherent scattering intensity on the basis of the formula for binary liquids.[26] The density of liquid under high-PT condition was estimated from the following three values: (i) the volume of the crystalline phase just before melting, (ii) the volume jump on melting,[27] (iii) the thermal expansion of the liquid.[28] The error of the number density was considered to be within 3 %.

We interpolated $S(Q)$ in the experimentally inaccessible Q region (below about 1 Å^{-1}) so that $S(Q)$ at the higher-Q region smoothly connect to the value at $Q=0$ Å^{-1}, $S(0)$, which is estimated from the number density and the isothermal compressibility. The effect of the interpolation on the profile of $g(r)$ was negligibly small, since $S(Q)$ in the low-Q region does not modify $g(r)$ significantly. Through these procedures, we obtained $S(Q)$ over Q region up to 15 Å^{-1}. We obtained $g(r)$ by the Fourier transformation of $S(Q)$, where we used the method described in Ref. 29 to minimize the error introduced in Fourier transformation. The structural information is summarized in Table I.

III. RESULTS

In Fig. 2, $S(Q)$ at high pressures are shown. We can see a characteristic hump ($Q \approx 3$–3.5 Å^{-1}) at high-Q side of the first peak throughout the pressure region of the present study.

TABLE I. Structural information of *l*-GaSb at high pressures.

										CN	
	P(GPa)	Q_1 (Å^{-1})	Q_2 (Å^{-1})	Q_2/Q_1	$S(Q_1)$	$S(Q_2)$	r_1 (Å)	r_2 (Å)	r_2/r_1	Disordered [a]	Ordered [b]
This study	1.7(1)	2.28	4.85	2.13	1.71	1.12	2.88	6.23	2.13	6.1(5)	6.5(5)
	3.0(1)	2.32	4.87	2.10	1.90	1.13	2.90	6.14	2.11	6.4(5)	6.8(5)
	3.6(1)	2.33	4.88	2.10	2.05	1.12	2.90	6.09	2.10	6.3(5)	6.7(5)
	4.3(1)	2.34	4.84	2.07	2.19	1.12	2.89	6.02	2.07	6.9(5)	7.3(5)
	4.7(1)	2.34	4.66	1.99	2.13	1.19	2.95	6.04	2.03	6.8(5)	7.2(5)
	5.4(1)	2.35	4.70	1.99	2.26	1.17	2.96	6.01	2.01	6.6(5)	7.0(5)
	5.5(1)	2.35	4.68	1.99	2.29	1.18	2.94	6.00	2.03	6.6(5)	7.0(5)
	8.3(1)	2.38	4.76	2.00	2.39	1.14	2.94	5.97	2.01	7.9(5)	8.4(5)
	10.1(1)	2.41	4.76	1.97	2.48	1.20	2.95	5.85	1.98	8.3(5)	8.8(5)
	11.7(2)	2.42	4.80	1.98	2.88	1.17	2.89	5.80	2.00	9.0(5)	9.5(5)
	16.7(3)	2.48	4.81	1.94	2.76	1.16	2.88	5.69	1.97	9.1(5)	9.6(5)
	19.6(3)	2.50	4.82	1.93	2.78	1.17	2.91	5.63	1.95	10.0(5)	10.6(5)
Estimated [c]	0.0									5.6(5)	5.9(5)
Previous study	0.0										5.4(5) [d]
	0.0										5.4 [e]

[a]CN for the chemically disordered model is calculated assuming $g_{\text{Ga-Ga}}=g_{\text{Sb-Sb}}=g_{\text{Ga-Sb}}$ (see text).
[b]CN for the chemically ordered model is calculated assuming $g_{\text{Ga-Ga}}=g_{\text{Sb-Sb}}=0$ in the first coordination shell (see text).
[c]The CN at ambient pressure is estimated by the extrapolation of the data between 1.7 and 8.3GPa assuming the linear relation between the pressure and the CN.
[d]Taken from Ref. 31.
[e]Taken from Ref. 32.

Near ambient pressure (1.7 GPa), the height of the first peak is found to be relatively small compared to that for simple liquids [$\approx$2.5–3.0] (Ref. 30). The ratio of the wave numbers of the second peak to the first peak, Q_2/Q_1, which is related to the anisotropy of the local structure in liquid, is much larger than that for simple liquids [$\approx$1.86] (Ref. 30). These features are commonly observed in previously reported $S(Q)$ of *l*-GaSb at ambient pressure.[31] With increasing pressure, the first peak and the hump continuously shift toward a higher-Q value, while the second and third peaks do not shift markedly. Consequently, Q_2/Q_1 ratio decreases with increasing pressure. Simultaneously, the height of the first peak increases and that of the hump decreases, while those for the second and third peaks do not change markedly. If liquids contract uniformly, $S(Q)$ would merely shift toward a lower-Q value without changing its profile. The observed changes suggest that *l*-GaSb contracts nonuniformly under pressure. Even by the compression up to 19.6 GPa, the hump still exists and the Q_2/Q_1 ratio is still larger than that for simple liquids. These imply the persistence of an anisotropic local structure in *l*-GaSb even by the compression up to 19.6 GPa.

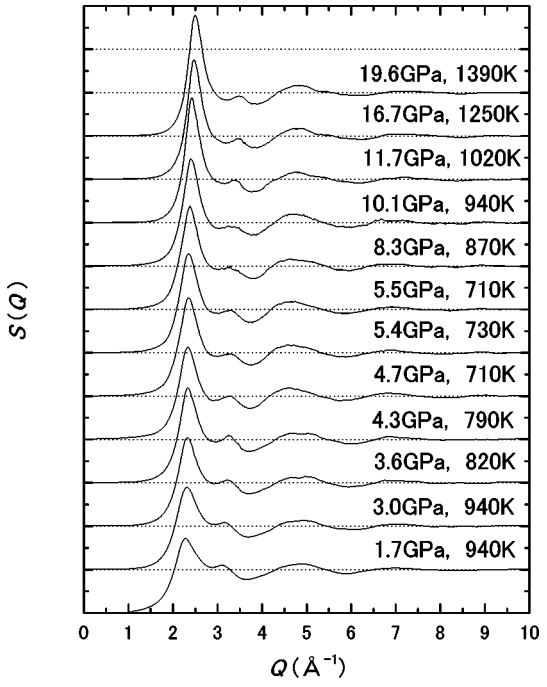

FIG. 2. $S(Q)$ of *l*-GaSb at high pressures.

In Fig. 3, $g(r)$ at high pressures are shown. We can see a characteristic hump ($r\approx$4.0 Å) at large r side of the first peak near ambient pressure. The trough between the first and second peaks is relatively shallow compared to that for simple liquids. The ratio in the position of the first peak to second peak in $g(r)$, r_2/r_1 ($\approx$2.13 at 1.7 GPa), is much larger than that for simple liquids [$\approx$1.84–1.90 (Ref. 30)]. These features are also observed in $g(r)$ of *l*-GaSb at ambient pressure[31] although a slight difference is observed in the position of the hump. With increasing pressure, the first peak does not shift markedly, while the other peaks and the hump shift toward smaller r values. No detectable change in the position of the first peak means that the nearest neighbor distance does not change markedly in spite of volume contraction. Simultaneously, the height of the second and third

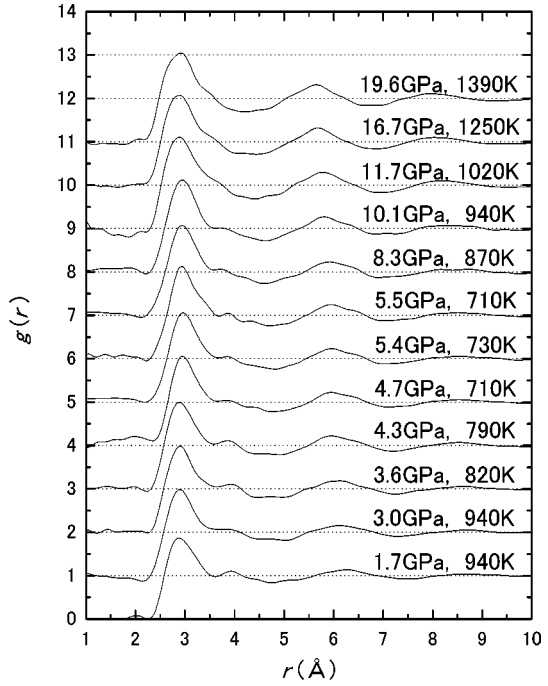

FIG. 3. $g(r)$ of *l*-GaSb at high pressures.

peaks increases and that of the hump decreases with pressure, while the height of the first peak does not change markedly with pressure. If liquid contracts uniformly, $g(r)$ would only shift toward a smaller r value without changing its profile. The observed changes in $g(r)$ suggest the nonuniform contraction of *l*-GaSb. The hump in $g(r)$ becomes smaller with increasing pressure, and it seems to be incorporated into the first peak above 11.7 GPa. Simultaneously, the trough between the first and second peaks becomes more prominent. These facts imply that the local structure of *l*-GaSb tends to lose the anisotropy with increasing pressure.

The coordination number CN of *l*-GaSb at high pressures is shown in Table I. We calculated the CN from radial distribution function RDF on the basis of the following equation:

$$\mathrm{CN_{RDF}}=2\int_{r_0}^{r_{\max}}4\pi r^2\rho_0 g(r)_{\mathrm{total}}dr. \tag{1}$$

Here, $g(r)_{\mathrm{total}}$ is total $g(r)$ in Faber-Ziman definition. The r_0 is the low-r limit of the first peak in RDF, and $r_{\max}$ is the r value at the top of the first peak in RDF. In their definition, the g_{total} is expressed by the sum of the partial pair distribution function of $g_{\mathrm{Ga\text{-}Ga}}$, $g_{\mathrm{Ga\text{-}Sb}}$, and $g_{\mathrm{Sb\text{-}Sb}}$ weighted by the concentration and atomic form factors,

$$g_{\mathrm{total}}=\frac{c_{\mathrm{Ga}}^2 f_{\mathrm{Ga}}^2}{\langle f\rangle^2}g_{\mathrm{Ga\text{-}Ga}}+\frac{2c_{\mathrm{Ga}}c_{\mathrm{Sb}}f_{\mathrm{Ga}}f_{\mathrm{Sb}}}{\langle f\rangle^2}g_{\mathrm{Ga\text{-}Sb}}+\frac{c_{\mathrm{Sb}}^2 f_{\mathrm{Sb}}^2}{\langle f\rangle^2}g_{\mathrm{Sb\text{-}Sb}}. \tag{2}$$

Here, c_{Ga} and c_{Sb} are the concentrations of Ga and Sb, respectively. The f_{Ga} and f_{Sb} are the atomic scattering factors for Ga and Sb, respectively, and $\langle f\rangle$ is the average one. In this definition, it is assumed that $f(Q)$ for each atom can be written by the universal $f(Q)_{\mathrm{uni}}$ function multiplied by the atomic number Z. The real CN should be calculated from the partial $\mathrm{CN_{i-j}}$. However, in the present study, we could not obtain the partial pair distribution functions $g_{\mathrm{Ga\text{-}Ga}}$, $g_{\mathrm{Ga\text{-}Sb}}$, and $g_{\mathrm{Sb\text{-}Sb}}$, and therefore, we could not obtain an exact CN. In this case, the CN calculated from RDF depends on the assumed model for the chemical short-range ordering. In the case for no tendency of pairing between Ga and Sb atoms (chemically disordered model), the g_{total} becomes equal to $g_{\mathrm{Ga\text{-}Ga}}$, $g_{\mathrm{Ga\text{-}Sb}}$, and $g_{\mathrm{Sb\text{-}Sb}}$ as long as the effect of the difference in the atomic diameter between two elements is not taken into account. Consequently, the CN directly calculated from RDF ($\mathrm{CN_{RDF}}$) becomes equal to the real one ($\mathrm{CN_{real}}$).

$$\mathrm{CN_{real}}=\mathrm{CN_{RDF}}. \tag{3}$$

On the other hand, in the case where the Ga (or Sb) tends to pair with the Sb (or Ga) atom (chemically ordered model) which corresponds to $g_{\mathrm{Ga\text{-}Ga}}=g_{\mathrm{Sb\text{-}Sb}}=0$ in the first coordination shell, the $\mathrm{CN_{real}}$ does not necessarily become equal to $\mathrm{CN_{RDF}}$. The $\mathrm{CN_{real}}$ for the ordered model is calculated from $\mathrm{CN_{RDF}}$ by the following equation under the condition of $c_{\mathrm{Ga}}=c_{\mathrm{Sb}}=0.5$:

$$\begin{aligned}\mathrm{CN_{real}}&=2\int_{r_0}^{r_{\max}}4\pi r^2 c_{Ga}\rho_0 g_{\mathrm{Ga\text{-}Sb}}(r)dr\\&=2\int_{r_0}^{r_{\max}}4\pi r^2 c_{Sb}\rho_0 g_{\mathrm{Sb\text{-}Ga}}(r)dr\\&=\frac{\langle f\rangle^2}{f_{\mathrm{Ga}}f_{\mathrm{Sb}}}\left[2\int_{r_0}^{r_{\max}}4\pi r^2\rho_0 g(r)_{\mathrm{total}}dr\right]\\&=\frac{\langle f\rangle^2}{f_{\mathrm{Ga}}f_{\mathrm{Sb}}}\mathrm{CN_{RDF}}.\end{aligned} \tag{4}$$

The CN calculated for both models is shown in Table I, where the uncertainty of CN for each model was estimated from the scatter of the data. Since the degree of ordering would be between these extreme cases practically, the CN would take a value between the values for these models. The results show that the CN at 1.7 GPa is 6.1/6.5 for the ordered/disordered models. This value is much smaller than 10-11 for simple liquids.[30] This fact implies that the local structure in *l*-GaSb is completely different from a simple one. With increasing pressure up to 19.6 GPa, the CN continuously increases up to 10.0/10.6 for the ordered/disordered models. The increase suggests that the local structure changes from a low-coordinated form into a more highly coordinated one with increasing pressure.

The CN at ambient pressure, which is estimated from the present data, was consistent with the value reported previously in Refs. 31 and 32 within an experimental uncertainty (Table I).

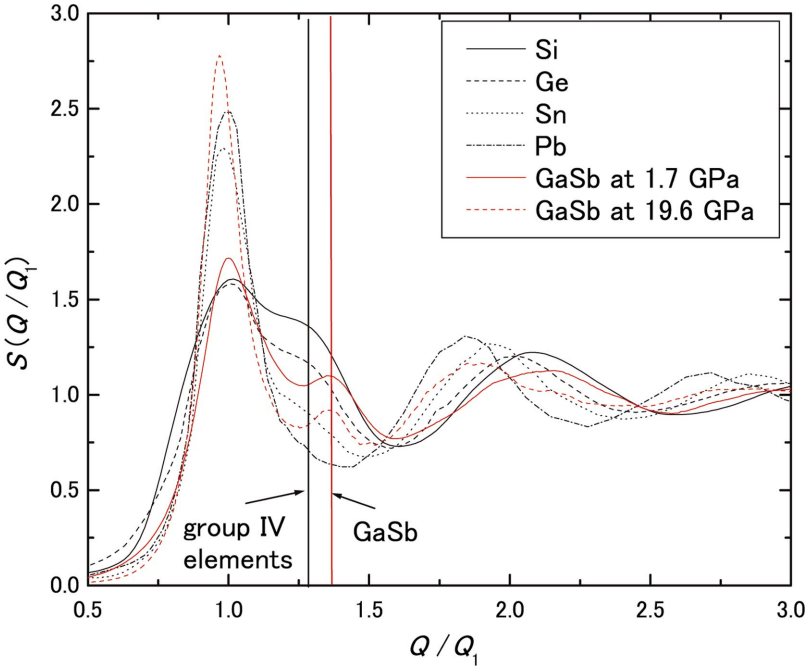

FIG. 4. (Color) $S(Q)$ for *l*-GaSb at 1.7 GPa and 19.6 GPa, and those for liquid group IV elements at ambient pressure (Ref. 30). The positions of the hump in $S(Q)$ for *l*-GaSb and for liquid group IV elements are shown by the vertical black and red lines, respectively.

IV. DISCUSSION

A. Structure of liquid

1. Comparison with simple liquids

The profile of $S(Q)$ for simple liquids is empirically known to have the following characteristics: (i) the profile has a simple oscillation (without any hump at high-Q side of the first peak), (ii) the height of the first peak is about 2.5–3.0 just above the melting temperature, (iii) $S(Q)$ has a marked trough between the first and second peaks, (iv) Q_2/Q_1 ratio is about 1.86.[30] The profile of $S(Q)$ for *l*-GaSb at 1.7 GPa is found to have the completely different characters from these ones: (i) $S(Q)$ has a hump at high-Q side of the first peak, (ii) the height of the first peak (≈ 1.7) is much smaller than that for simple liquids, (iii) the trough between the first and second peaks is considerably small, (iv) Q_2/Q_1 ratio (≈ 2.13) is much larger than that for simple liquids. These suggest that the local structure of *l*-GaSb is not simple near ambient pressure. These characters are also observed in *l*-Si and *l*-Ge.[33,34] Therefore, an anisotropic local structure originating in the residual covalent character is also considered to exist in *l*-GaSb.

With increasing pressure, the deviation from simple liquids becomes smaller. It is obvious from the following pressure-induced changes: (i) the decrease in the height of the hump, (ii) the increase in the height of the first peak, (iii) the growth of the trough between the first and second peaks, (iv) the decrease in Q_2/Q_1 ratio. These characters imply that the local structure in *l*-GaSb gradually loses the anisotropy and that the liquid approaches a simple one with increasing

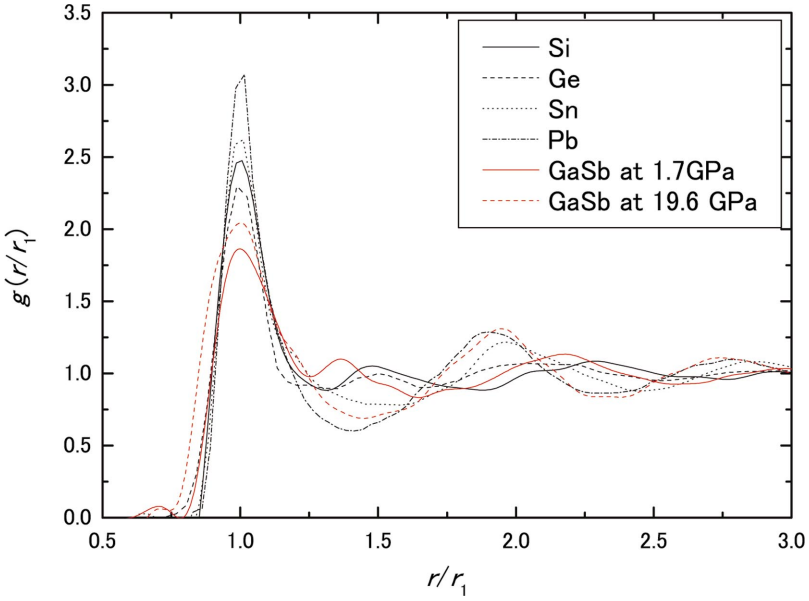

FIG. 5. (Color) Comparison of $g(r)$ between *l*-GaSb at 1.7 GPa and 19.6 GPa, and those for liquid group IV elements at ambient pressure (Ref. 30).

pressure. However, the aforementioned characters are still observed at 19.6 GPa, which suggests that the anisotropic local structure persists up to 19.6 GPa in some amount.

The same conclusion is also obtained from $g(r)$. It is known that $g(r)$ for simple liquids have the following characteristics: (i) $g(r)$ shows a simple oscillation without any hump peak (ii) the trough between the first and second peaks is prominent, (iii) the ratio in the position between the first and second peaks, r_2/r_1, is 1.84–1.90.[30] The profile of $g(r)$ for *l*-GaSb near ambient pressure (1.7 GPa) is also found to has the different characters from these ones: (i) $g(r)$ has a hump at a large r side of the first peak, (ii) the trough between the first and second peaks is less prominent, (iii) r_2/r_1 value ($\approx$2.13 at 1.7 GPa) is much larger than that for simple liquids. These different characters support that *l*-GaSb has a nonsimple local structure.

With increasing pressure, the deviation of $g(r)$ from that for simple liquids becomes smaller; namely, (i) the hump becomes smaller, (ii) the trough becomes more prominent, (iii) r_2/r_1 ratio becomes smaller. These pressure dependences suggest that the local structure of *l*-GaSb approaches a simple one with increasing pressure. When we assume that an anisotropic local structure originates in the covalent character in chemical bonds, *l*-GaSb is considered to lose the covalent character gradually with increasing pressure.

2. Comparison with liquid group IV elements

The previously mentioned characters in $S(Q)$ for *l*-GaSb are also observed in liquid group IV elements, especially, in the liquid phase of the lighter element. The following tendency is observed as descending from Si to Pb in IV column. (See Fig. 4): (i) the height of the hump becomes smaller, (ii) the height of the first peak becomes larger, (iii) the trough between the first and second peaks becomes more prominent, (iv) Q_2/Q_1 ratio becomes smaller. These features suggest that the liquid of the lighter element has the larger anisotropy in the local structure. This is reasonable because the anisotropy is considered to originate in the covalent character and it becomes larger in the lighter element.[35] When we compare the pressure dependence of $S(Q)$ for *l*-GaSb with that of the atomic number dependence in liquid group IV elements, a similar tendency is observed: the pressure increase corresponds to the increase of the atomic number. It is widely known that the heavier group IV elements have weaker covalent character, so *l*-GaSb is considered to lose the covalent characters with increasing pressure. This feature is physically plausible because the increase of the pressure, and the resultant increase of the electron density, induces the overlap of the wave function between atoms, which contributes to metallic bonding. The similar tendency also suggests that with increasing pressure the local structure in *l*-GaSb changes from the one similar to that of a light-element liquid into that of the heavy-element liquid.

When we compare $S(Q)$ of liquid group IV elements with that for *l*-GaSb in more details, a slight but significant difference is observed. The $S(Q)$ of liquid group IV elements[30] and of *l*-GaSb (at 1.7 GPa and 19.6 GPa) are shown in Fig. 4. Each profile is normalized by the position of the first peak. In the figure, $S(Q)$ for *l*-GaSb at other pressures is not shown because $S(Q)$ continuously changes from that at 1.7 GPa into that at 19.6 GPa with increasing pressure. The normalized wave number of the hump in $S(Q)$ for *l*-GaSb is found to be about 1.39, regardless of pressure. On the other hand, the corresponding value for liquid group IV elements is about 1.30, regardless of the chemical species. The difference between these values cannot be attributed to the difference in the pressure condition, because the normalized wave number of the hump, Q_{hump}/Q_1, is almost independent of the pressure, as is evident from the pressure dependence of the hump position for *l*-GaSb. The difference implies that the local structure for *l*-GaSb is somehow different from those for liquid group IV elements. This may be related to the difference in the ionicity of the chemical bonding between GaSb and group IV elements, or may be attributed to the existence of two chemical species with the different atomic diameters in *l*-GaSb.

In Fig. 5, $g(r)$ for liquid group IV elements[30] and those for *l*-GaSb at 1.7 GPa and 19.6 GPa are shown. Here, each profile is normalized at the position of the first peak. The $g(r)$ for *l*-GaSb at other pressures are not shown because of the same reason described in the comparison of $S(Q)$. In $g(r)$ for liquid group IV elements, the following atomic number dependencies are observed as descending from Si to Pb in column: IV (i) the hump becomes smaller, (ii) the trough between the first and second peaks becomes more evident, (iii) the height of all the peaks except the hump becomes larger, (iv) the r_2/r_1 ratio becomes smaller. This tendency means that the liquid with the heavier element is closer to simple liquids.

When we compare the above-mentioned tendency with the pressure dependence of $g(r)$ for *l*-GaSb, a similar tendency is observed. This supports the idea that *l*-GaSb gradually loses its covalent character with increasing pressure. Furthermore, the similarity of $g(r)$ for *l*-GaSb at 19.6 GPa to that for liquid Sn (*l*-Sn) implies that the local structure of *l*-GaSb approaches that in *l*-Sn with pressure.

B. Pressure dependence of the structure

Previously, the structures of *l*-Si and *l*-Ge have been investigated up to 23 GPa and 25 GPa, respectively.[5,6] The following pressure-dependence is observed in $S(Q)$ for *l*-Si and *l*-Ge: With increasing pressure, (i) the height of the hump becomes smaller, (ii) the height of the first peak increases, (iii) the trough between the first and second peaks becomes more prominent, (iv) Q_2/Q_1 ratio becomes smaller. These dependencies are the same as those observed in *l*-GaSb. This implies that the pressure-induced modification of local structure for *l*-GaSb is qualitatively the same as those for *l*-Si and *l*-Ge.

However, when we compare the pressure dependence quantitatively in more details, we find the marked difference in the pressure range where the hump exists. The hump becomes less prominent above 14 GPa in *l*-Si (Ref. 5) and above 18 GPa in *l*-Ge.[6] On the other hand, the hump is still evident even at 20 GPa in *l*-GaSb. In crystalline states, the transition pressure is empirically known to become lower for the materials with the larger atomic number. On the basis of

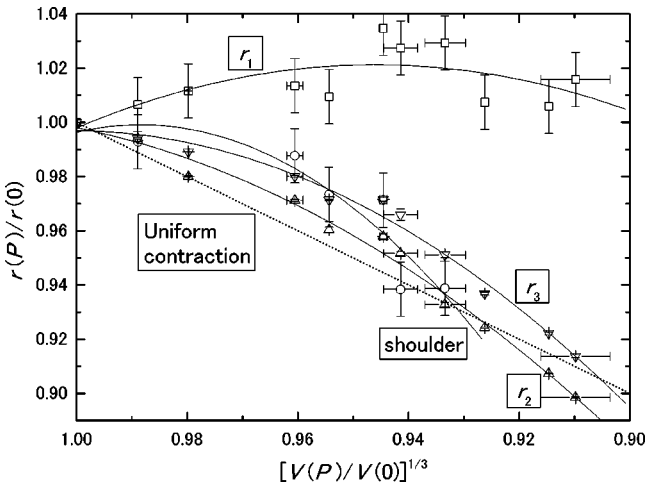

FIG. 6. Normalized position of the peaks in $g(r)$, $r_i(P)/r_i(0)$, at high pressures as a function of $[V(P)/V(0)]^{1/3}$. The r_1, r_2, and r_3 mean the positions for the first, second, and third peaks in $g(r)$, respectively. These values are determined by the Gaussian fitting of the $g(r)$ in the r region with $g(r) > 1 + 9/10\ (g_{max} - 1)$ for r_1 and in the r region with $g(r) > 1$ for r_2 and r_3, where g_{max} means the height of the first peak. The uniform contraction model is shown by the dotted line. The thin lines are only guide for the eye.

this empirical rule, the hump of *l*-GaSb should become less prominent at the lower pressure than *l*-Si and *l*-Ge. The persistence of the hump at the anomalously high pressure in *l*-GaSb supports the idea that the origin of the hump in $S(Q)$ for *l*-GaSb is somehow different from those for *l*-Si and *l*-Ge.

C. Contraction process

1. Comparison with simple liquids

In order to elucidate the contraction process of *l*-GaSb, the peak positions in $g(r)$ are shown against the cube root of the volume which corresponds to the average interatomic distance (Fig. 6). Here, each value is normalized by the respective value at ambient pressure.[36] For comparison, the line for the uniform contraction model is also shown. We find that the pressure dependence of the first peak deviates largely from the line for the uniform contraction, while those of the second and third peaks lie approximately along the line. This clearly shows that *l*-GaSb contracts nonuniformly. This behavior is completely different from the high-pressure behavior for liquid alkali metals.[37]

Since the position of the first peak corresponds to the nearest-neighbor distance, the above result means that the nearest-neighbor distance does not change significantly in spite of the volume contraction. From the pressure dependence of the first peak and that of the mean atomic distance, it can be said that the nearest-neighbor distance *increases* with increasing pressure. This picture is supported by the fact that the pressure-induced increase in the CN, which is usually accompanied with the increase of the nearest-neighbor distance, is simultaneously observed in the present study. The apparent constancy in the nearest-neighbor distance under pressure, as previously notified, would be explained as the result of the cancellation between the decrease of the nearest neighbor distance by compression and the increase of it by the gradual change of the local structure from a low-pressure form with the smaller nearest-neighbor distance into a high-pressure form with the larger one.[38] The cancellation by this mechanism is actually found to occur in *l*-GaSb from the results of the local structure analysis of *l*-GaSb as shown later in Sec. IV D.

2. Comparison with c-GaSb

To compare the contraction behaviors between the liquid and crystalline states is important for knowing the effect of the disorder in the atomic arrangement on the contraction. The following phases are reported in *c*-GaSb in the pressure region below 20 GPa: the zinc-blende structure, the site-disordered β-Sn structure,[14,15] the orthorhombic *Imma* phase,[17] and the orthorhombic *Ammm* phase.[4] All these phases are considered to show a uniform or an almost uniform contraction. For example, the zinc-blende structure contracts uniformly by the application of hydrostatic pressure. The orthorhombic *Imma* phase, which has the degree of freedom in two axial ratios (b/a and c/a) and an internal coordinate, is known to contract almost uniformly without the significant change in these parameters.[17] Although the contraction process for GaSb with these structures has not been reported yet, the site-disordered β-Sn and orthorhombic *Ammm* phases are also expected to contract uniformly from the results for Ge.[39] The uniform contraction in *c*-GaSb is natural because the chemical bonding in these structures, which is the sp^3 hybrid bonding and/or the metallic bonding, does not have dispersion of the bond strength in the chemical bonds.

Contrary to the crystalline phases, *l*-GaSb shows a nonuniform contraction. Two mechanisms can be considered as an origin of the nonuniform contraction. One is the deformation of the local structure under pressure. In liquid states, the wide variation in bond length and bond angle is allowed due to the absence of the periodicity. Therefore, the local structure can be easily deformed by the variation of the bond length and bond angle under pressure. The other mechanism is the change in the ratio of several local structures coexisting in liquid states. As expressed by two-species model (TSM),[40] *l*-GaSb may consist of a mixture of several local structures. When $S(Q)$ and $g(r)$ for each local structure are different from each other and the mixing ratio of the local structure changes with pressure, $S(Q)$ and $g(r)$, which comprise $S(Q)$ and $g(r)$ for each local structure, also change with pressure. In such case, the liquid shows the apparently nonuniform contraction. The nonuniform contraction of *l*-GaSb is considered to be caused by this mechanism from the results of the local structure analysis as shown in the following subsection.

D. Estimation of the local structure

Previous studies on liquid group IV elements have suggested that the local structure in the liquids is similar to those in the high-pressure crystalline phases.[7,33,41,42] Since *l*-GaSb is denser than zinc-blende-type GaSb at ambient pressure as liquid group IV elements are, the same idea may be appli-

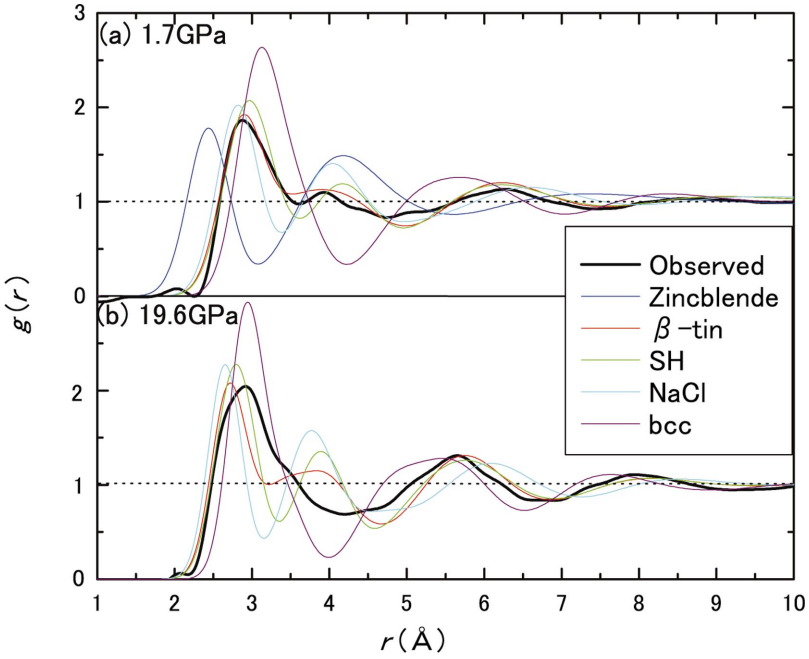

FIG. 7. (Color) Experimental $g(r)$ and simulated one for several crystal structures: (a) at 1.7 GPa and (b) at 19.6 GPa.

cable for *l*-GaSb. In order to estimate the local structure of *l*-GaSb, we compared the experimentally determined $g(r)$ with those simulated from the crystal structures reported previously in group IV elements and III-V compounds. To take the similarity of short-range order between liquid and crystalline states into account, we have simulated $g(r)$ for liquid by giving a Gaussian-type bond-length distribution to $g(r)$ for the crystalline phases (distorted crystalline model: See Sec. 1 of the Appendix).

In binary liquids, the chemical short-range order also modifies the profile of $S(Q)$ and $g(r)$. In the simulation, *l*-GaSb is assumed to have no chemical ordering because of the small ionic character of *l*-GaSb.[43] Even in the case that *l*-GaSb had a complete chemical ordering, the effect on the profile of $S(Q)$ and $g(r)$ was found to be negligible due to the small difference in the x-ray atomic scattering factor between Ga and Sb.

We first compared the experimental $g(r)$ with those simulated from a single local structure in several crystalline phases (single-species model). Next, we considered the possible coexistence of two local structures (TSM). This idea was originally postulated by Klement[40] and was extended by Rapoport using statistical mechanics to explain the melting curve maxima under pressure.[1] In Rapoport's model, the fraction of two species are quantitatively related to the external parameters *P* and *T*. Hereafter, we call his model ''Rapoport's TSM'' to distinguish it from Klement's TSM. The validity of Rapoport's TSM is confirmed by the good agreement of the experimental electric properties with those calculated on the basis of the model.[44,45]

1. Analysis by the single-species model

First of all, we examined the possible existence of the local structure similar to the crystalline phases previously reported in *c*-GaSb. The profile of $g(r)$ for the liquid with each local structure were simulated by the distorted crystalline model. The lattice parameters for each structure was estimated from the number density of *l*-GaSb at high pressures.[46] In the simulation of $g(r)$ for the β-Sn-like, the SH-like, and the orthorhombic *Imma*-like local structures, we used the previously reported structural parameters, such as the axial ratios and the internal coordinates.[4,16,17] When the simulated $g(r)$ could not successfully reproduce the experimental $g(r)$, we modified these parameters.

The typical results of the analysis are shown in Fig. 7. The $g(r)$ for the orthorhombic *Imma*-like and *Ammm*-like structures are not shown because $g(r)$ for these structures are almost the same as those for the β-Sn-like and SH-like structures, respectively. The simulated $g(r)$ for the zinc-blende-like structure does not reproduce the experimental $g(r)$ at 1.7 GPa in terms of the presence of the hump and the positions of the peaks. On the other hand, $g(r)$ for the β-Sn-like structure successfully reproduces the general features of the experimental $g(r)$ at 1.7 GPa. This suggests that the local structure of *l*-GaSb at 1.7 GPa is close to the site-disordered β-Sn structure, rather than the zinc-blende structure. This is not so surprising because *l*-GaSb is considered to consist of the denser local structure than the zinc-blende-like one at ambient pressure.

Although $g(r)$ simulated for the β-Sn-like structure reproduces the general features of the experimental $g(r)$ at 1.7 GPa, the slight differences are still observed in the position of the peaks and the hump. The difference could not be improved even when we use another axial ratio. The change of the axial ratios of c/a and b/a and the internal coordinates from those for the β-Sn structure, which corresponds to the simulation using the orthorhombic *Imma* structure, does not improve the fitting results. It may imply that *l*-GaSb cannot be described by a single local structure.

When we compare the experimental $g(r)$ at 19.6 GPa with that simulated from the zinc-blende structure, a marked difference is observed. Even when we use the β-Sn-like lo-

cal structure in the simulation, the large difference is observed both in the position of the peaks and the height of the hump. This suggests that *l*-GaSb at 19.6 GPa cannot be described by the β-Sn-like local structure anymore, and that the local structure of the liquid changes from the β-Sn-like one into another one with increasing pressure. Since the experimental $g(r)$ and $S(Q)$ change continuously with increasing pressure, the change of the local structure is considered to be gradual.

To check the possible existence of another local structure except the high-pressure crystalline phases of GaSb, we compared $g(r)$ with those simulated for the crystal structures reported previously in group IV elements and other III-V compounds. The following other structures have been previously reported in Si, Ge, Sn, AlSb, GaAs, GaP, InAs, and InP in the pressure region below 30 GPa: a bcc structure, a body-centered tetragonal (bct) structure, an orthorhombic *Cmcm* structure, and NaCl-type structure.[3,39,47–54] The results of the comparison are shown in Fig. 7. The $g(r)$ simulated for the bct and the orthorhombic *Cmcm* structures are not shown because $g(r)$ for these structures are almost the same as those for bcc and NaCl-type structures, respectively. The $g(r)$ simulated for any crystal structures could not reproduce the experimental $g(r)$. All these analyses using the single-species model could not explain the experimental $g(r)$ at 19.6 GPa. However, when we see the results of the comparison more carefully, we find that the experimental $g(r)$ at 19.6 GPa is close to the profile averaged between those for the β-Sn-like and bcc-like structures over whole r region up to 10 Å. Furthermore, when we compare the experimental $g(r)$ at other pressures with the simulated ones, we find the experimental one goes through the intersection points of the $g(r)$'s for β-Sn and bcc-like local structures. This implies the possibility that the experimental $g(r)$ is expressed by the linear combination of those $g(r)$'s simulated for these two crystal structures.

2. Analysis by the TSM

Motivated by the above-mentioned results, we analyzed $g(r)$ assuming that the liquid consists of a mixture of two local structures similar to those observed in crystalline phases. This does not necessarily mean the existence of two microcrystallines, but means the existence of two kinds of the short-range orders similar to those observed in the crystalline phases.

We simulated $g(r)$ for the liquid with two local structures similar to those in crystalline phases on the basis of the formulas shown in Sec. 2 of the Appendix. As for two crystal structures, various pairs are used from those realized in group IV elements and III-V compounds, which are already mentioned in the preceding section. To fit the experimental $g(r)$ by the simulated one, we employed the following parameters: (i) the number density ρ_0, which determines the lattice parameters for each structure, (ii) σ_1 and t, which determine the dispersion for the Gaussian, (iii) the fraction of the high-pressure form, x. We determined these parameters by minimizing the average difference R between the observed and calculated $g(r)$:

$$R=\sqrt{\frac{1}{N}\sum_{i=0}^{N-1}\{g_{obs}(r_i)-g_{calc}(r_i)\}^2}. \tag{5}$$

Here, r_0 and r_{N-1} are respectively, taken as 2.2 Å [the low-r limit of the first peak in $g(r)$] and 10.0 Å. Results of the fitting are shown in Fig. 8 and Table II. We obtained a fairly good agreement between the experimental and simulated $g(r)$ when we used the pair of the β-Sn and bcc structures, rather than the pair of the zinc-blende and β-Sn structures which are the stable crystalline phases in the pressure range of the present study. By using TSM, the fitting is improved compared to that using the single-species model. The fraction for the β-Sn-like and bcc-like local structures at high pressures is shown in Fig. 9 and Table II, where the uncertainty of the fraction is estimated from the residuals of the fitting. The fraction for β-Sn-like local structure continuously decreases and that for the bcc-like one increases with increasing pressure. This indicates that the local structure of *l*-GaSb gradually changes from the β-Sn-like structure into the bcc-like one with increasing pressure. This view is consistent with the experimentally observed increase in the CN from about 6 at 1.7 GPa to about 10 at 19.6 GPa because the continuous change of the local structure causes the continuous increase of the CN from $4+2$ (Ref. 55) for the β-Sn-like one into $6+8$ (Refs. 55 and 56) for the bcc-like one.

When we assume that the pressure-induced change of the local structure is continuous, we can estimate the fraction of the bcc-like local structure at ambient pressure by the extrapolation of the data at pressures below 4.3 GPa. The results show that the fractions for the β-Sn-like and bcc-like local structures are, respectively, 1.00 ± 0.04 and 0.00 ± 0.04 at ambient pressure. This implies that *l*-GaSb can be described only by the β-Sn-like local structure at ambient pressure.

In *l*-GaSb, the liquid-liquid phase transition with the discontinuous volume change at 4–8 GPa, depending on temperature, was suggested from the results of thermobaric analysis[57] and from the discontinuous change in the slope of the melting curve.[11] The present result shows a slight jump of the fraction of the high-pressure form, x, between 4.3 GPa and 4.7 GPa, although the uncertainty of x is comparable to the jump. The liquid-liquid phase transition reported in Ref. 57 may be related to the discontinuous change of the local structure from the β-Sn-like one into bcc-like one.

In the analysis using TSM, the existence of bcc-like local structure which has not been reported in *c*-GaSb was confirmed. The existence of the bcc-like local structure in liquid state can be understood by either of the following two mechanisms. One is the appearance as a result of the lowering of transition pressure from β-Sn-like into the bcc-like local structures in the liquid state due to the preference of the coexisting state originating from mixing entropy.[58] The other mechanism is the appearance of the simple-liquid metals, rather than the bcc-like local structure. It is found that $g(r)$ simulated for the bcc-like-local structure with the distortion successfully explains $g(r)$ for simple liquids. Therefore, the expression of the experimental $g(r)$ by a mixture with the bcc-like local structure may imply the existence of

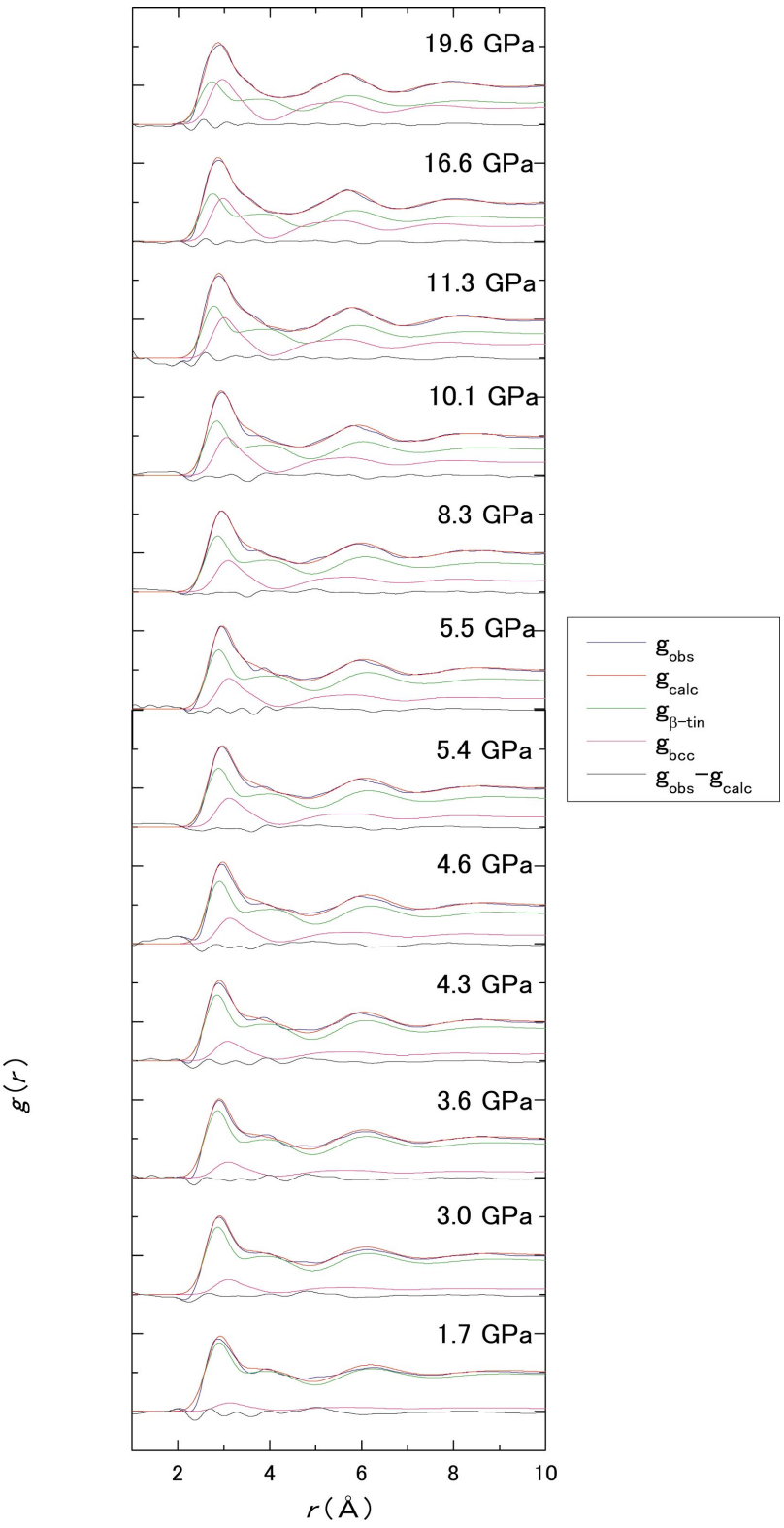

FIG. 8. (Color) Experimental and simulated $g(r)$ for *l*-GaSb at high pressures. The profile of $g(r)$ is simulated by the linear combination of $g(r)$ for the β-Sn-like and bcc-like structures, where $g(r)$ for each structure is weighted by the fractional ratio. The difference between the experimental and simulated $g(r)$ is also shown.

the simple-liquid-like structure. The same coexistence of the covalent (β-Sn-like) local structure and the metallic (bcc-like) one is also suggested by Kōga and Yonezawa[7] for *l*-Ge on the basis of the simulation studies.

E. Application of Rapoport's TSM

To understand the change of the local structure more quantitatively, we analyzed the experimentally determined PT dependence of the fraction of the high-pressure form by

TABLE II. Fraction of the β-Sn-like and bcc-like local structures at high pressures and the reliable factor for the fitting, R

	Fraction		
P (GPa)	β-Sn	bcc	R
1.7(1)	0.92(1)	0.08(1)	0.06
3.0(1)	0.86(1)	0.14(1)	0.05
3.6(1)	0.85(1)	0.15(1)	0.05
4.3(1)	0.82(1)	0.18(1)	0.05
4.7(1)	0.77(1)	0.23(1)	0.06
5.4(1)	0.74(1)	0.26(1)	0.04
5.5(1)	0.73(1)	0.27(1)	0.04
8.3(1)	0.71(1)	0.29(1)	0.04
10.1(1)	0.66(1)	0.34(1)	0.05
11.7(2)	0.64(1)	0.36(1)	0.05
16.7(3)	0.60(1)	0.40(1)	0.03
19.6(3)	0.57(1)	0.43(1)	0.04

Rapoport's TSM.[1] In his model, the fraction of the high-pressure form, x, is related to the pressure and temperature by the following equation:

$$k_B T \ln\frac{x}{1-x} + (1-2x)w = \Delta\mu^0 \quad (\Delta\mu^0 = \Delta\epsilon^0 - T\Delta S^0 + P\Delta V^0). \tag{6}$$

Here, k_B is a Boltzmann constant and w is the energy needed for the replacement of a like pair of the local structures with an unlike pair. The parameters $\Delta\mu^0$, $\Delta\epsilon^0$, ΔS^0, and ΔV^0 are the differences in the chemical potential, internal energy, entropy, and volume between the low- and high-pressure forms, respectively. These parameters are assumed to be independent of the pressure and the temperature. First, we determined these parameters through the fitting of the fractions of the high-pressure form by this model. Next, we draw the isofraction lines for the high-pressure form in PT space on the basis of the parameters obtained by the fitting.

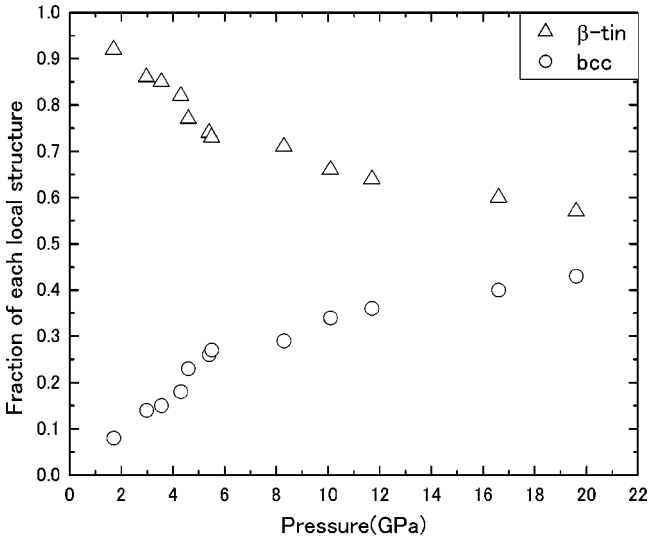

FIG. 9. Fraction for the β-Sn-like and bcc-like local structures in l-GaSb at high pressures.

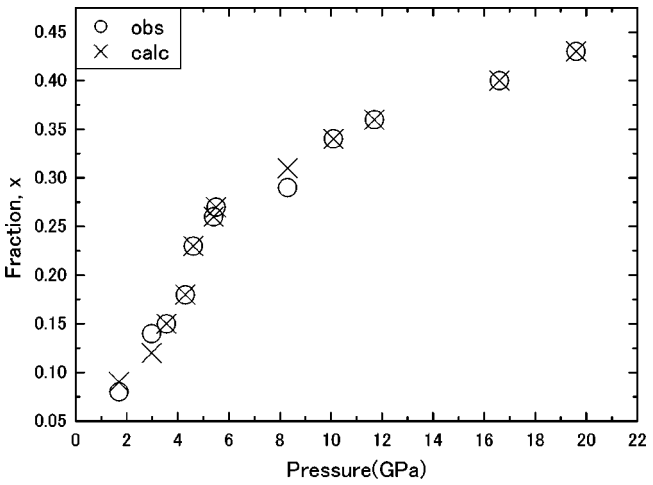

FIG. 10. Results of the fitting of the PT dependence of the fraction for the high-pressure form by Rapoport's TSM. The refined parameters are shown in Table III.

The result of the fitting is shown in Fig. 10. The PT dependence of the fraction of the high-pressure form is successfully explained by Rapoport's TSM, which supports the applicability of TSM to l-GaSb. The following values are determined by the fitting: $\Delta\epsilon^0 = 1.1\times10^{-20}$ J/atom, $\Delta V^0 = 2.5$ Å^3/atom, $\Delta S^0 = 4.7\times10^{-23}$ $(=3.4k_B)$ J/K per atom, $w = 1.3\times10^{-21}$ $(=0.091k_BT$ at $T=1000$ K) J/atom. These parameters are found to be consistent with available data. The value of ΔV^0 is expected to take a similar value to the volume difference between the β-Sn-type GaSb and bcc-type GaSb [$\approx$1.5–2.2 Å^3/atom. (Ref. 59)] The experimentally determined value ($\Delta V^0 = 2.5$ Å^3/atom) is found to agree with this value within the experimental uncertainty. In Rapoport's TSM model, the liquid with the larger w value than 2.0 k_BT tends to separate into the low- and high-density liquids. Since we did not observe the phase separation in this study, w should be smaller than $2.0k_BT$. The experimentally determined w value ($w = 0.091k_BT$ at $T=1000$ K) satisfies this condition.

The isofraction lines for the bcc-like local structure, which are calculated using the above-mentioned parameters, are shown in Fig. 11. At ambient pressure and the temperature just above the melting point, most part of the liquid consists of the β-Sn-like local structure. With increasing pressure and decreasing temperature, the fraction of the β-Sn-like local structure decreases and that of bcc-like one increases continuously.

F. Pressure-induced change of the local structure

1. Comparison with c-GaSb

When we compare the local structures and the pressure-induced structural change between l-GaSb and c-GaSb, we find several marked differences. One of the differences is the pressure interval for the structural change. The local structure gradually changes over wide pressure region in l-GaSb,

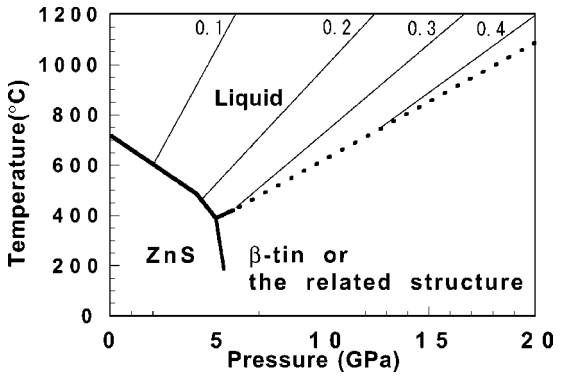

FIG. 11. Iso fraction lines calculated for bcc-like local structure in PT plane for *l*-GaSb. Phase boundary is drawn in the same way as shown in the caption of Fig. 1.

while the local structure suddenly changes at a certain pressure in *c*-GaSb. The wide pressure interval for the liquid would be related to the large stability of the coexisting state of the several local structures in liquid. This can be understood in terms of two points. One is the small interfacial energy at the boundary region between two local structures in liquid states. When several local structures coexist, the potential energy increases due to the mismatch of the bond length and bond angle at the boundary region. However, the liquid state can avoid it by the slight modification in the geometry of each local structure with the help of the flexibility in the bond length and bond angle. On the other hand, the crystalline states can not avoid it because the local structure cannot change the bond length and bond angle freely due to the restriction of the translational symmetry. The second reason is the large mixing entropy for liquid state with several local structures. At high temperature, the entropy term $-TS$ plays an important role as well as the potential and the PV terms. When we consider the entropy of mixing several local structures, it would be much larger in liquid states than in crystalline states since the various arrangements of the local structure are possible in liquid states due to the wide distribution of the bond length and bond angle. From the above-mentioned reasons, the liquid with several local structures is considered to be stabilized because the gain of the free energy by mixing several local structures is larger than the increase of the interfacial energy caused by the bond disorder. On the other hand, the crystalline phase with several local structures is not possible due to the less gain in free energy by mixing than the increase of the interfacial energy.

Another difference between *l*-GaSb and *c*-GaSb is the pressure where the structural change starts. Now, we think that both states take basically the same high-pressure sequence in the local structures from the zinc-blende structure, which is considered to exist at (imaginary) negative pressure in *l*-GaSb, into the β-Sn-like and/or the related structures, and then into the bcc-like local structure. However, the pressure range showing this sequence shifts toward the lower pressure in *l*-GaSb compared to *c*-GaSb. For example, the first structural change (from the zinc-blende structure into the β-Sn one) has already completed at ambient pressure and the second change (from the β-Sn structure into the bcc one) starts at about 0–2 GPa in *l*-GaSb, while the first change occurs at 6–7 GPa and the second one does not start even by the compression up to 35 GPa in *c*-GaSb. This difference may be related to the difference of the stability of each local structure in the liquid state and in the crystalline state. When we compare the aforementioned three structures, the structure becomes less tolerant for the bond angle variation in the order of the bcc, β-Sn, and zinc-blende structures, due to more covalent (less metallic) character in the chemical bonds. Since in liquid states, the bond angle is widely distributed due to the large atomic movements and no constraints for periodicity, the liquid would tend to prefer the local structure which is tolerant for the bond angle variation, such as the bcc-like or the β-Sn-like local structure. Because of this reason, the β-Sn-like and bcc-like local structures are considered to be observed at much lower pressure in *l*-GaSb.

2. Comparison with l-Si

In *l*-Si, it is reported that the local structure changes drastically within a relatively narrow pressure range. This behavior is considerably different from that of *l*-GaSb, in which the local structure gradually changes over a wide pressure region. Although the detailed mechanism of the drastic change in *l*-Si is still unknown, the different behavior may be explained by the anomalously narrow stable pressure range for the β-Sn-like local structure in *l*-Si compared to that in *l*-GaSb. It is reported that the crystalline Si shows the following high-pressure sequence in the pressure range below 30 GPa: the diamond structure transforms into β-Sn structure at 12 GPa, and then into the orthorhombic *Imma* phase at 13 GPa, and then into the SH structure at 16 GPa.[47,49,50,53] This sequence is typical among the tetrahedrally bonded materials, such as Ge and other III-V compounds. However, the stable pressure range for the β-Sn and the related *Imma* phases is known to be anomalously narrow in Si ($\approx$4 GPa) compared to Ge [$\approx$70 GPa (Refs. 39 and 60)] and GaSb [$\approx$13 GPa (Ref. 4)]. Assuming that the local structure changes in the similar way to crystalline phases, *l*-Si may drastically change its local structure from a low-pressure form into another high-pressure one (probably SH structure) passing through the β-Sn-like local structure since the stable region for the β-Sn phase is narrow.

3. Comparison with liquid Cs (l-Cs) and liquid Te (l-Te)

The pressure dependence of the fraction for the high-pressure form has been investigated for *l*-Cs and *l*-Te.[44,45] Compared to these results, it is found that much higher pressure is required for the complete conversion from the low-pressure form into the high-pressure one in *l*-GaSb. Actually, the application of the pressure of about 20 GPa only induced the change of the fraction from 0.0 to about 0.5 for *l*-GaSb, while the application of only 5 GPa and 1.5 GPa is large enough for the almost complete conversion for *l*-Cs and *l*-Te, respectively. This difference can be understood by the small values of ΔV^0 and w for *l*-GaSb. The conversion rate of the local structure at the constant T is expressed by[1]

TABLE III. Parameters of Rapoport's TSM for *l*-GaSb, *l*-Cs, and *l*-Te.

Material	$\Delta\epsilon^0$ (J/atom)	ΔV^0 (Å^3/atom)	ΔS^0 (J/Kper atom)	ω (J/atom)	$\frac{\omega}{k_B T}$
l-GaSb [a]	1.1×10^{-20}	2.5	4.7×10^{-23}	1.3×10^{-21}	0.091[b]
l-Cs [c]	-2.0×10^{-20}	5.7	-7.0×10^{-24}	1.0×10^{-20}	1.5[b]
l-Te [d]	2.9×10^{-22}	2.5	1.1×10^{-24}	2.0×10^{-20}	2.01[b]

[a]This study.
[b]The values for *l*-GaSb, *l*-Cs, and *l*-Te are calculated at the temperatures of 1000 K, 493 K, and 737 K, respectively.
[c]Recalculated using the parameters in Ref. 44.
[d]Recalculated using the parameters in Ref. 45.

$$\left(\frac{\partial x}{\partial P}\right)_T = \frac{\frac{\Delta V^0}{k_B T}}{\frac{1}{x(1-x)} - 2\frac{w}{k_B T}}. \tag{7}$$

At $x=0.5$, the value takes a maximum

$$\left(\frac{\partial x}{\partial P}\right)_T (\text{at } x=0.5) = \frac{\frac{\Delta V^0}{k_B T}}{4 - 2\frac{w}{k_B T}}. \tag{8}$$

This value becomes a good scale for measuring the conversion rate. Small values of ΔV^0 and w lead to the gradual change of the local structure. The comparison of these values (Table III) reveals that ΔV^0 and w for *l*-GaSb are in fact smaller than those for *l*-Cs and *l*-Te, and explains gradual change of local structure for *l*-GaSb against pressure.

G. Origin of the hump of $S(Q)$

From the analysis of the local structure, we have estimated the origin of the hump in $S(Q)$ for *l*-GaSb. The comparison of the experimental $S(Q)$ at 1.7 GPa and 19.6 GPa with those simulated for the β-Sn-like and bcc-like structures weighted by the determined fraction is shown in Figs. 12(a) and 12(b). Here, the horizontal axis is scaled by the position of the first peak. The comparisons of $S(Q)$ at other pressures are not shown because similar results are obtained. We can find that the hump in the experimental $S(Q)$ comes from that of $S(Q)$ for the β-Sn-like local structure both at 1.7 GPa and 19.6 GPa. This implies that the hump in $S(Q)$ for *l*-GaSb originates in the β-Sn-like local structure at any pressure.

As already shown in Fig. 4, the normalized position of the hump for liquid group IV elements is slightly deviated from that for *l*-GaSb. Consequently, the position of the hump of $S(Q)$ for the β-Sn-like local structure does not show a good agreement with that for liquid group IV element. To explain the origin of the hump for liquid group IV elements, we need to consider the large deformation from the β-Sn-like local structure or the existence of another local structure.

H. Contraction mechanism

1. Contraction of l-GaSb

As already mentioned, two main mechanisms are considered for a nonuniform contraction of liquids. One is the nonuniform contraction originating in the deformation of the local structure due to the dispersion in the strength of the chemical bonds. The other is the nonuniform contraction originating in the pressure-induced change in the fraction of the several local structures. The nonuniform contraction observed in *l*-GaSb is considered to be caused by the latter mechanism.

In the present study, the nonuniform contraction in *l*-GaSb is confirmed from an anisotropic change of the profiles of $S(Q)$ and $g(r)$ under pressure and the different pressure dependence in the positions of the first, second, and third peaks in $g(r)$. As evident in Fig. 7, the profiles of $S(Q)$ and $g(r)$ are different between the β-Sn-like and bcc-like local structures. Since the total $S(Q)$ and $g(r)$ are expressed by the linear combination of those for two local structures, the pressure-induced change of the fraction causes the modification of $S(Q)$ and $g(r)$ under pressure. The different pressure dependence of peak positions is also explained by this mechanism. As shown in Fig. 7, each peak position in $g(r)$ is different between the β-Sn-like and bcc-like local structures. Therefore, when the fraction of the local structure changes with pressure, the positions of first, second, and third peaks in $g(r)$ also show the different pressure dependence. The aforementioned two evidences for the non-uniform contraction of *l*-GaSb can be explained by the pressure-induced change in the fraction of the high-pressure form. Therefore, the nonuniform contraction in *l*-GaSb is considered to be caused by the gradual change of the local structure from the β-Sn-like one and bcc-like one under pressure.

2. Comparison with liquid group IV elements

It is reported that *l*-Si contracts uniformly in the pressure region below 8 GPa and above 14 GPa.[5] However, *l*-Si also seems to contract nonuniformly because Q_2/Q_1 value, which is expected to be constant regardless of pressure for the uniform contraction, changes with pressure. In *l*-Ge, the profiles for $S(Q)$ and $g(r)$ also change with increasing pressure, together with the change of Q_2/Q_1 ratio.[6] These results

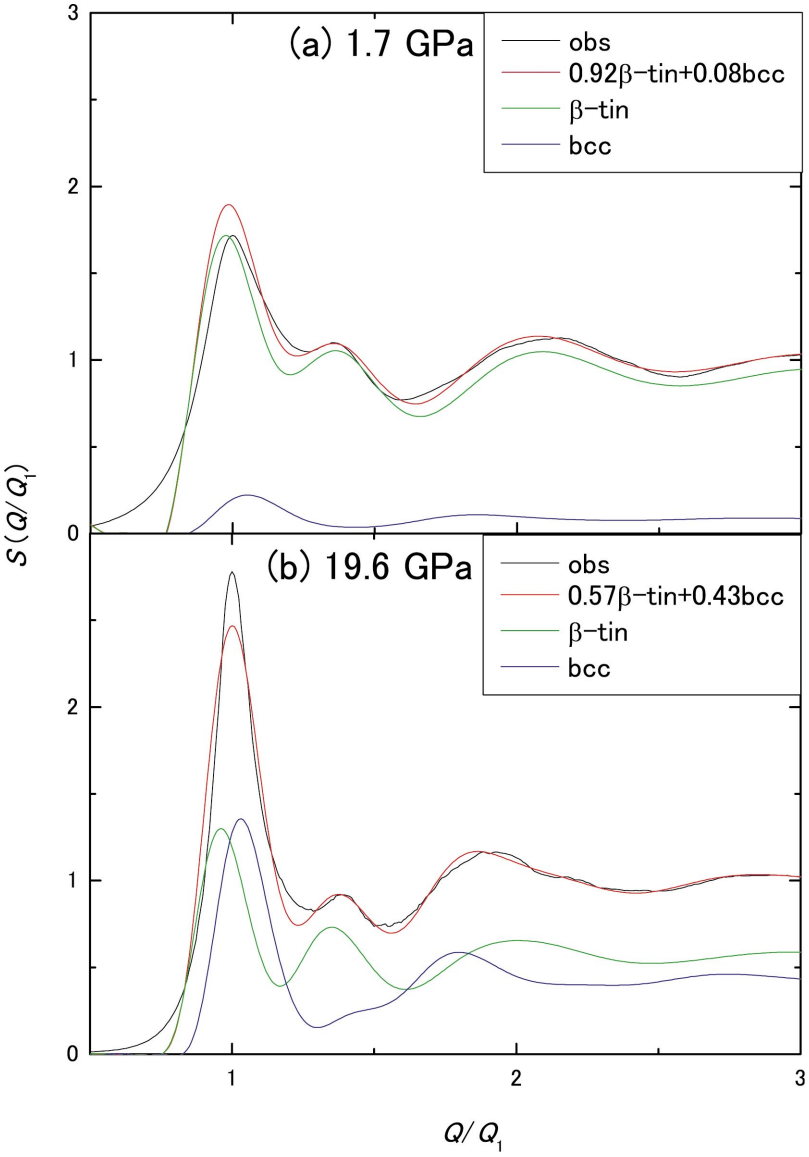

FIG. 12. (Color) Experimental $S(Q)$ for l-GaSb (a) at 1.7 GPa and (b) at 19.6 GPa and the simulated $S(Q)$ for the β-Sn-like and bcc-like structures weighted by the fractional ratio. The horizontal axis is normalized by the wave number of the first peak Q_1. The profile of $S(Q)$ which is generated by the linear combination of those for the β-Sn-like and bcc-like structures is also shown.

suggest that both liquids show a nonuniform contraction similar to that for l-GaSb. Although the detailed contraction mechanisms for these liquids are still unknown, these liquids are also considered to contract nonuniformly through the pressure-induced change in the fraction of the high-pressure local structure by considering the similarity of Si and Ge to GaSb in the nature of the chemical bond and the high-pressure sequences in the crystalline phases. Though, the detailed mechanism of the contraction for these liquids should be investigated through the quantitative analysis of the local structure.

3. Comparison with the liquids with a low-dimensional network

Previously, the contraction processes of liquid chalcogen and liquid Halogen have been investigated.[6,9,61–63] These liquids form a low-dimensional network due to the small CN. These liquids are also known to contract nonuniformly under pressure. The mechanism of the nonuniform contraction for these liquids, however, seems to be different from that for l-GaSb.

The liquid chalcogens, such as liquid Se (l-Se) and l-Te, consist of one-dimensional chains. Each atom is tightly bonded to two neighbors within a chain by the covalent bonds, while each chain is bonded to the adjacent chains by much weaker bond. With increasing pressure, the weaker intrachain bond contracts selectively. The nonuniform contraction of the liquid chalcogen is considered to be caused by the anisotropic contraction of the local structure.

The similar contraction mechanism is applicable for liquid halogen.[6] The liquid Iodine consists of the molecule of the paired atoms. Each atom is tightly bonded to a neighbor atom with the covalent bonding, while the molecules are loosely bonded to each other by a much weaker bond. With increasing pressure, the weaker intermolecular bond contracts selectively. The nonuniform contraction in liquid iodine is also caused by the anisotropic contraction of the local structure. As observed in these examples, the liquids with a low-dimensional network contract nonuniformly due to the dispersion in the strength of the chemical bonds. This mechanism is completely different from that of nonuniform con-

traction in the liquid of tetrahedrally bonded materials with less dispersion in the strength of the chemical bonds.

V. CONCLUSION

In order to elucidate the local structure and the pressure-induced change for the liquids of tetrahedrally bonded materials, we have investigated the structure of *l*-GaSb at high pressures up to 20 GPa by synchrotron x-ray-diffraction measurements. We have revealed the contraction process of *l*-GaSb from the precisely determined $g(r)$. We also identified the local structure and its pressure-induced change by applying the distorted-crystalline model and TSM to the experimental $g(r)$ *quantitatively*. We also applied Rapoport's TSM to the PT dependence of the fraction of the high-pressure form from the experimental $g(r)$. These results were compared with those for *c*-GaSb, liquid group IV elements, and the liquid with a low-dimensional network. The main results of this study are listed below.

(i) The *l*-GaSb contracts nonuniformly, which is completely different from a uniform contraction for simple liquids.

(ii) The local structure of *l*-GaSb is described by the mixture of the local structures (β-Sn-like and bcc-like local structures) similar to the high-pressure phases of *c*-GaSb, rather than that similar to an ambient form, zinc-blende structure. The fraction of the high-pressure form continuously increases as the pressure is raised.

(iii) Two local structures coexist over a wide pressure region below 20 GPa.

(iv) The local structures of the high-pressure phases observed in *c*-GaSb (β-Sn-like and bcc-like local structures) appear at much lower pressure in *l*-GaSb.

(v) The pressure and temperature dependence of the local structures is successfully explained by Rapoport's TSM.

ACKNOWLEDGMENTS

We thank N. Funamori, T. Kikegawa, K. Funakoshi, W. Utsumi, and O. Shimomura for an experimental assistance. We thank F. Yonezawa, H. Okumura, J. Koga, and K. Nishio for valuable discussions. We also thank Y. Saito for proofreading the manuscript. This work was performed under the approval of the Photon Factory Program Advisory Committee (No. 2000G044) and of the Japan Synchrotron Radiation Research Institute (JASRI) (Nos. 2000B0087 and 2001B0472).

APPENDIX

1. Method for simulating $g(r)$ for liquids: Distorted crystalline model

It is natural to consider that a short-range order in liquid states is similar to those in the crystalline states. Taking this into consideration, we simulate $g(r)$ for the liquid from that for the crystalline phase.

The pair distribution function $g(r)$ for a crystalline phase is expressed by

$$g_{\mathrm{crystal}}(r)=\frac{1}{4\pi r^2\rho_0}\sum_{i=1}^{N}\delta(r-r_i), \tag{A1}$$

where r_i is the interatomic distance to ith atom from the atom centered at origin, N is the number of atoms, and ρ_0 is the average number density. For the preservation of the number of atoms, $g_{\mathrm{crystal}}(r)$ satisfies the following condition:

$$\int_0^{\infty}4\pi r^2\rho_0 g_{\mathrm{crystal}}(r)dr=N. \tag{A2}$$

In the simulation of $g(r)$ for liquid, we give a Gaussian-type fluctuation to the interatomic distance for expressing the wide distribution in the bond length and bond angle in liquid. The contribution of the jth atom at a distance r_{j} to $g(r)$ is expressed by

$$g_{\mathrm{j}}(r)=\frac{A_{\mathrm{j}}}{\sqrt{2\pi}\sigma_{\mathrm{j}}}e^{-(r-r_{\mathrm{j}})^2/2\sigma_{\mathrm{j}}^2}, \tag{A3}$$

where σ_{j} is the dispersion of the Gaussian distribution for jth atom, and A is a scaling factor. The factor is determined from the following condition for the preservation of the number of an atom:

$$\int_0^{\infty}4\pi r^2\rho_0 g_{\mathrm{j}}(r)dr=1. \tag{A4}$$

By solving this equation, we obtain the following scaling factor:

$$A_{\mathrm{j}}=\frac{1}{4\pi\rho_0(r_{\mathrm{j}}^2+\sigma_{\mathrm{j}}^2)}. \tag{A5}$$

In order to include the gradual decrease in the short-range order with the increase of the interatomic distance, the dispersion of the Gaussian, σ_{j}, is enlarged with the increase of the interatomic distance:

$$\sigma_{\mathrm{j}}=\left(\frac{r_{\mathrm{j}}}{r_1}\right)^t\sigma_1. \tag{A6}$$

Here, r_1 is the interatomic distance of the nearest-neighbor atom, and σ_1 is the dispersion of the Gaussian for the atom.

We obtain $g(r)$ for liquid by the summation of the $g_{\mathrm{j}}(r)$ over all atoms, as shown by the following equation:

$$g(r)=\sum_{j=1}^{N}g_{\mathrm{j}}(r). \tag{A7}$$

The similar methods have been reported previously in Refs. 64 and 65. Compared to the formula in Ref. 64, the parameter t is kept as a variable in this study. It is because this parameter can not be determined *a priori* due to the uncertainty of the decay rate for the order in the bond length and in bond angle. Compared to the formulas in Ref. 65, the scaling factor A_{j} is improved in our formulas because the number of atoms is not preserved in their formula.

2. Method for simulating $g(r)$ for the liquids with two local structures: TSM

Generally, $g(r)$ for the liquid with two constituents of the low- and high-pressure forms (LPF and HPF) is expressed by

$$g(r)=(1-x)^2 g_{\text{LPF-LPF}}(r)+x^2 g_{\text{HPF-HPF}}(r) + 2x(1-x)g_{\text{LPF-HPF}}(r). \quad \text{(A8)}$$

Here, x is the fraction of the HPF, and $g_{\text{LPF-LPF}}(r)$, $g_{\text{HPF-HPF}}(r)$, and $g_{\text{LPF-HPF}}(r)$ are the partial $g(r)$ for the pair between LPF's, HPF's, and LPF-HPF, respectively. When we assume that the partial $g(r)$ between different forms is expressed by the average of the partial $g(r)$'s between the same forms as

$$g_{\text{LPF-HPF}}(r)=\frac{g_{\text{LPF-LPF}}(r)+g_{\text{HPF-HPF}}(r)}{2}, \quad \text{(A9)}$$

the total $g(r)$ is expressed by the linear combination of $g(r)$ for the same forms:

$$g(r)=(1-x)g_{\text{LPF-LPF}}(r)+xg_{\text{HPF-HPF}}(r). \quad \text{(A10)}$$

On the basis of these formulas, we can obtain a total $g(r)$ for the liquid with two local structures.

Here, even if the approximation expressed by Eq. (A9) is not correct, the general feature of formula (A10) does not change so much regardless of the model used. For example, if the different forms do not have any short-range order, i.e., $g(r)$ between different forms is constant independent of r, the total $g(r)$ can be expressed by

$$g(r)=(1-x)^2\ \ g_{\text{LPF-LPF}}(r)+x^2 g_{\text{HPF-HPF}}(r)+2x(1-x). \quad \text{(A11)}$$

Even in this case, $g(r)$ can be expressed by the combination of $g_{\text{LPF-LPF}}(r)$ and $g_{\text{HPF-HPF}}(r)$ although the coefficient is not a linear one. In another case, if $g_{\text{LPF-HPF}}(r)$ is expressed by the linear combination of $g_{\text{LPF-LPF}}(r)$ and $g_{\text{HPF-HPF}}(r)$ with a different weight y as shown by the following equation,

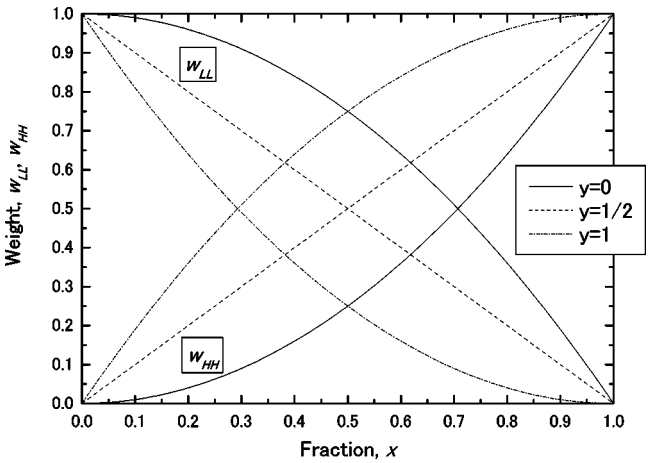

FIG. 13. Weight factors for $g_{\text{LPF-LPF}}$ (w_{LL}) and for $g_{\text{HPF-HPF}}$ (w_{HH}) as function of the fraction of the high-pressure form, x, for the model of $y = 0, 1/2, 1$ (see text).

$$g_{\text{LPF-HPF}}(r)=(1-y)\ \ g_{\text{LPF-LPF}}(r)+y\ \ g_{\text{HPF-HPF}}(r), \quad \text{(A12)}$$

the $g(r)$ can be expressed by

$$g(r)=w_{\text{LL}}g_{\text{LPF-LPF}}(r)+w_{\text{HH}}g_{\text{HPF-HPF}}(r), \quad \text{(A13)}$$

$$w_{\text{LL}}=(1-x^2)-2x(1-x)y, \quad \text{(A14)}$$

$$w_{\text{HH}}=x^2+2x(1-x)y. \quad \text{(A15)}$$

Here, w_{LL} and w_{HH} are the weights for $g_{\text{LPF-LPF}}(r)$ and $g_{\text{HPF-HPF}}(r)$, respectively. In the case of $y=0$, which corresponds to $g_{\text{LPF-HPF}}(r)=g_{\text{LPF-LPF}}(r)$, w_{LL} and w_{HH} become $(1-x^2)$ and x^2, respectively. In the case of $y=1$, which corresponds to $g_{\text{LPF-HPF}}(r)=g_{\text{HPF-HPF}}(r)$, w_{LL} and w_{HH} become $(1-x)^2$ and $1-(1-x)^2$, respectively. In any cases, the $g(r)$ can be expressed by the combination of $g_{\text{LPF-LPF}}(r)$ and $g_{\text{HPF-HPF}}(r)$, while the coefficients are slightly modified. In Fig. 13, the dependences of w_{LL} and w_{HH} against x are shown for the models of $y=0, 1/2, 1$.

[1] E. Rapoport, J. Chem. Phys. **46**, 2891 (1967).
[2] Y. Katayama, T. Mizutani, W. Utsumi, O. Shimomura, M. Yamakata, and K. Funakoshi, Nature (London) **403**, 170 (2000).
[3] M.I. McMahon and R.J. Nelmes, J. Phys. Chem. Solids **56**, 485 (1995), and references therein.
[4] C.B. Vanpeteghem, R.J. Nelmes, D.R. Allan, and M.I. McMahon, Phys. Rev. B **65**, 012105 (2001).
[5] N. Funamori and K. Tsuji, Phys. Rev. Lett. **88**, 255508 (2002).
[6] T. Mori, Master thesis, Keio University, 2000.
[7] J. Kōga and F. Yonezawa, Phys. Rev. B **66**, 064211 (2002).
[8] J.C. Phillips, *Bonds and Bands in Semiconductors* (Academic Press, New York, 1973).
[9] N. Funamori and K. Tsuji, Phys. Rev. B **65**, 014105 (2001).
[10] W. Utsumi, K. Funakoshi, S. Urakawa, Y. Yamakata, K. Tsuji, H. Konishi, and O. Shimomura, Rev. High Pressure Sci. Technol. **7**, 1484 (1998).
[11] D. Martínez-Garcia, Y.L. Godec, G. Syfosse, and J.P. Itié, Phys. Status Solidi B **211**, 475 (1999).
[12] A. Jayaraman, W. K., Jr., and G.C. Kennedy, Phys. Rev. **130**, 540 (1963).
[13] H.P. Mokrovskii and A.R. Regel, J. Tech. Phys. **22**, 1282 (1952).
[14] J.C. Jamieson, Science **139**, 845 (1963).
[15] C. Yu and I.L. Spain, Solid State Commun. **25**, 49 (1978).
[16] S.T. Weir, Y.K. Vohra, and A.L. Ruoff, Phys. Rev. B **36**, 4543 (1987).
[17] M.I. McMahon, R.J. Nelmes, N.G. Wright, and D.R. Allan, Phys. Rev. B **50**, 13 047 (1994).
[18] M. Mezouar, H. Libotte, S. Deputier, T.L. Bihan, and D. Häusermann, Phys. Status Solidi B **211**, 395 (1999).
[19] K. Tsuji, K. Yaoita, M. Imai, O. Shimomura, and T. Kikegawa, Rev. Sci. Instrum. **60**, 2425 (1989).
[20] The diffraction profiles were taken at $2\theta=3°$, $4°$, $5°$, $6°$, $8°$,

10°, 12°, 15°, and 20° for the experiments using the MAXIII apparatus, and at $2\theta = 3°$, 4°, 5°, 6°, 8°, 11°, and 15° for the experiment using the SPEED1500 apparatus.

[21] D.L. Decker, J. Appl. Phys. **42**, 3239 (1971).

[22] The intensity of liquid in the subtracted region was estimated by interpolating the data in the lower- and higher-Q regions by a third polynomial function.

[23] J.A. Ibers and W. Hamilton, *International tables for X-ray crystallography* (Kynoch, Birmingham, UK, 1974), Vol. IV.

[24] D.T. Cromer and J.B. Mann, J. Chem. Phys. **47**, 1892 (1967).

[25] D.T. Cromer, J. Chem. Phys. **50**, 4857 (1969).

[26] T.E. Faber and J.M. Ziman, Philos. Mag. **11**, 153 (1965).

[27] We estimated the volume jump on melting at high pressures from that at ambient pressure and the slope of melting curve on the basis of Clausius-Clapeyron relation. Here, we assumed that the entropy change on melting is independent of pressure in the pressure range of the present study.

[28] The thermal-expansion coefficient of the liquid was assumed to be equal to that of the crystalline phase before melting at each pressure. The error caused by this assumption is negligibly small because the contribution of the thermal expansion to the number density is small (within 1%).

[29] R. Kaplow, S.L. Strong, and B. Averbach, Phys. Rev. **138**, 1336 (1965).

[30] Y. Waseda, *The Structure of Non-Crystalline Materials* (McGraw-Hill, New York, 1980).

[31] J. Mizuki, K. Kakinoki, M. Misawa, T. Fukunaga, and N. Watanabe, J. Phys.: Condens. Matter **5**, 3391 (1993).

[32] Y. Wang, K. Lu, and C. Li, Phys. Rev. Lett. **79**, 3664 (1997).

[33] Y. Waseda and K. Suzuki, Z. Phys. B **20**, 339 (1975).

[34] J.P. Gabathuler and S. Steeb, Z. Naturforsch. **A34**, 1314 (1979).

[35] W.A. Harrison, *Electronic Structure and the Properties of Solids* (Freemann and Company, San Francisco, 1980).

[36] We calculated the positions of the peaks at ambient pressure by extrapolating the respective values at high pressures toward ambient pressure.

[37] Y. Morimoto, S. Kato, N. Toda, Y. Katayama, K. Tsuji, K. Yaoita, and O. Shimomura, Rev. High Pressure Sci. Technol. **7**, 245 (1998).

[38] The gradual increase of the nearest-neighbor distance is likely to occur in liquids because two characteristic distances for the low- and high-pressure forms cannot be divided in liquids because of the large distribution of the bond length.

[39] Y.K. Vohra, K.E. Brister, S. Desgreniers, A.L. Ruoff, K.J. Chang, and M.L. Cohen, Phys. Rev. Lett. **56**, 1944 (1986).

[40] W. Klement (unpublished).

[41] V. Petkov, S. Takeda, Y. Waseda, and K. Sugiyama, J. Non-Cryst. Solids **168**, 97 (1994).

[42] Y. Waseda, K. Shinoda, K. Sugiyama, S. Takeda, and K. Terashima, Jpn. J. Appl. Phys., Part 1 **34**, 4124 (1995).

[43] C.B. Vanpeteghem, R.J. Nelmes, D.R. Allan, M.I. McMahon, A.V. Sapelkin, and S.C. Bayliss, Phys. Status Solidi B **223**, 405 (2001).

[44] E. Rapoport, Phys. Rev. Lett. **19**, 345 (1967).

[45] E. Rapoport, J. Chem. Phys. **48**, 1433 (1968).

[46] We calculated the lattice parameters for each local structure from the volume of the liquid which does not involve the volume jump on melting to avoid the overestimation of the interatomic distance for the local structures in liquids. It is because the volume jump on melting is considered to originate from the formation of voids in liquid, rather than from the abrupt increase of the interatomic distance.

[47] J.C. Jamieson, Science **139**, 762 (1963).

[48] J.D. Barnett, R.B. Bennion, and H.T. Hall, Science **141**, 1041 (1963).

[49] H. Olijnyk, S.K. Sikka, and W.B. Holzapfel, Phys. Lett. **103A**, 137 (1984).

[50] J.Z. Hu and I.L. Spain, Solid State Commun. **51**, 263 (1984).

[51] S. Desgreniers, Y.K. Vohra, and A.L. Ruoff, Phys. Rev. B **39**, 10 359 (1989).

[52] C.A. Vanderborgh, Y.K. Vohra, and A.L. Ruoff, Phys. Rev. B **40**, 12 450 (1989).

[53] M.I. McMahon and R.J. Nelmes, Phys. Rev. B **47**, 8337 (1993).

[54] M.I. McMahon and R.J. Nelmes, Phys. Status Solidi B **198**, 389 (1996).

[55] The coordination number for the β-Sn structure is counted as $4+2$ because the first coordination shell cannot be distinguished from the second one due to the small difference in the distance (within 5%). Similarly, the coordination number for the bcc structure is counted as $8+6$.

[56] The experimentally determined coordination number at 19.6 GPa is not equal to the value for the bcc structure $(6+8)$ because the change of the local structure is not completed at 19.6 GPa.

[57] A.G. Umnov, J. Phys.: Condens. Matter **6**, 4625 (1994).

[58] Although the bcc-type GaSb has not been reported in *c*-GaSb in the pressure region below 35 GPa, the phase is expected to exist at the pressure much higher than 35 GPa because Sn and InSb, which have a similar electronic structure to GaSb, have the bcc-type higher-pressure crystalline phase (Refs. 48 and 52).

[59] We calculated the volume difference between the β-Sn-type and bcc-type structures for GaSb with reference to that for Sn, because the bcc-type GaSb has not been reported yet. In the calculation, we assumed that the ratio of the volume jump to the volume of the parent phase at the transition pressure is identical between GaSb and Sn. The following data are used in the calculation: $V_{\text{zinc-blende}} = 28.54$ Å^3/atom, $V_{\beta\text{-Sn}} = 23.31$ Å^3/atom for GaSb (Ref. 16), and $V_{\text{zinc-blende}} = 34.154$ Å^3/atom, $V_{\beta\text{-Sn}} = 27.05$ Å^3/atom (Ref. 66 and 67), $V_{\text{bcc}} = 25.293$ Å^3/atom (Ref. 48) for Sn. By using these data, we calculated the volume difference between the β-Sn type and bcc-type structures for GaSb as 1.5–2.2 Å^3/atom.

[60] R.J. Nelmes, H. Liu, S.A. Belmonte, J.S. Loveday, M.I. McMahon, D.R. Allan, D. Häusermann, and M. Hanfland, Phys. Rev. B **53**, R2907 (1986).

[61] K. Tsuji, J. Non-Cryst. Solids **117-118**, 27 (1990).

[62] Y. Katayama, K. Tsuji, H. Kanda, H. Nosaka, K. Yaoita, T. Kikegawa, and O. Shimomura, J. Non-Cryst. Solids **205-207**, 451 (1996).

[63] Y. Katayama, T. Mizutani, W. Utsumi, O. Shimomura, and K. Tsuji, Phys. Status Solidi B **223**, 401 (2001).

[64] J. Sietsma and B.J. Thijsse, J. Non-Cryst. Solids **101**, 135 (1988).

[65] V. Petkov, A. Apostolov, and V. Skumryev, J. Non-Cryst. Solids **110**, 184 (1989).

[66] JCPDS no. 4-0673.

[67] JCPDS no. 5-0390.